published by Ural Federal University
eISSN 2411-1414
chimicatechnoacta.ru

ARTICLE
2024, vol. 11(4), No. 202411402
DOI: 10.15826/chimtech.2024.11.4.02

Green synthesis of $CdFe_2O_4$ by *Terminalia catappa* leave extract for photodegradation methyl red dye by response surface methodology

Poedji Loekitowati Hariani [a*], Salni [b], Eka Sri Yusmartini [c], Nabila Aprianti [d], Bijak Riyandi Ahadito [a]

a: Research Group on Magnetic Materials, Department of Chemistry, Faculty of Mathematics and Natural Sciences, Universitas Sriwijaya, Ogan Ilir 30662, Indonesia
b: Department of Biology, Faculty of Mathematics and Natural Sciences, Universitas Sriwijaya, Ogan Ilir 30662, Indonesia
c: Chemical Engineering Department, Faculty of Engineering, Universitas Muhammadiyah, Palembang 30263, Indonesia
d: Research Centre for Energy Conversion and Conservation (PRKKE), National Research and Innovation Agency (BRIN), B.J. Habibie Science and Technology Park, South Tangerang 15314, Indonesia
* Corresponding author: puji_lukitowati@mipa.unsri.ac.id

This paper belongs to a Regular Issue.

Abstract

Green synthesis using plant extracts is an eco-friendly approach that reduces the hazards associated with chemical usage. This study aimed to synthesize a $CdFe_2O_4$ ferrite compound utilizing *Terminalia catappa leaves* extract and evaluate its photocatalytic efficiency in degrading Methyl red dye. The X-ray diffraction (XRD) analysis confirms the synthesis of $CdFe_2O_4$, which has a crystallite size mean of 18.10 nm. The composite exhibits magnetic properties with a saturation magnetization of 28.34 emu/g, a band gap of 1.78 eV, and a BET surface area of 84.23 m^2/g. The optimal photodegradation process was determined using Response Surface Methodology (RSM) based on an experiment with Central Composite Design (CCD). The variables examined included the solution pH, the initial concentration of the dye, and the irradiation time. The interplay of three variables demonstrated their reciprocal influence on photodegradation efficiency. The quadratic model is appropriate for modeling the photodegradation of Methyl red dye. The photodegradation efficiency of 96.56% is achieved under optimal conditions, which include a pH of 6.33, an initial dye concentration of 39.93 mg/L, and an irradiation time of 52.26 min. Empirical investigations on the reusability of $CdFe_2O_4$ have shown remarkable stability. Experimental kinetics confirm that the pseudo-first-order model is a suitable description for the photodegradation of Methyl red dye by $CdFe_2O_4$.

Keywords

$CdFe_2O_4$
Green synthesis
Terminalia Catappa L
Methyl red dye
RSM

Received: 31.07.24
Revised: 20.08.24
Accepted: 28.08.24
Available online: 13.09.24

Key findings

- The green synthesis method can be used to synthesize of $CdFe_2O_4$ using *Terminalia catappa* L leave extract.
- Optimization of photodegradation By RSM shows that the quadratic model is suitable for describing the photodegradation of Methyl red dye using $CdFe_2O_4$.
- $CdFe_2O_4$ can be regenerated and used repeatedly for photodegradation.

1. Introduction

Industries such as textiles, pulp, paper, leather, cosmetics, dyes, food packaging, plastics, and food and pharmaceutical chemicals frequently employ organic dyes for the purpose of coloring [1–3]. Most dyes utilized in industrial applications are azo dyes, which contain N=N bond [4]. Azo dyes possess inherent toxicity and exhibit a poor degradation mechanism, hence being classified as environmentally hazardous [5, 6]. Discharged dyes build up in organisms,

reducing the dissolved oxygen in the water and harming aquatic life [7]. Methyl red dye is one example of an azo dye. Apart from its industrial applications, laboratory settings also utilize this dye as an acid-base indicator. Methyl red dye exhibits mutagenic, mitotic, toxic, and carcinogenic properties [8, 9]. Hence, it is crucial to eliminate the dye from wastewater to its disposal into the environment.

Several methods have been developed to remove Methyl red dye, including adsorption [8], bioelectricity [9], membrane separation [10], microbial electrochemical [11], and photocatalytic degradation [12]. Among these, photocatalysis is the most effective method for degrading dye, as it converts dye constituents into CO_2, H_2O, and harmless by-products, thereby preventing secondary pollution [13]. When the catalyst is exposed to radiation, electrons are excited from the valence band to the conduction band, causing the creation of an electron hole-pair (e^--h^+). This pair triggers a reaction that produces hydroxyl radicals ($^{\bullet}OH$) and superoxide radical anions ($^{\bullet}O_2^-$ **),** which will degrade the dye on the surface near the catalyst [14, 15].

Spinel ferrites are p-type semiconductors that are widely used as photocatalysts. The chemical formula is MFe_2O_4, where M (Cu, Mg, Ni, Co, Zn, Cd, etc.) is a divalent ion in either octahedral or tetrahedral. On the other hand, Fe is a trivalent ion located in an octahedral position [16, 17]. Many researchers have employed spinel ferrite as a catalyst for breaking down dyes, such as $MgFe_2O_4$ [18], $CdFe_2O_4$ [19], Fe_3O_4 [20], and $CoFe_2O_4$ [21].

Various methods can be employed to synthesize ferrite compounds, such as precipitation [22], solution combustion [23], sonochemistry [24], and green synthesis [25]. The green synthesis approach offers several advantages over alternative methods, including its ecologically conscious nature, cost-effectiveness, rapid and straightforward synthesis process, low energy usage, and scalability [26, 27]. Numerous studies have utilized plant extracts, such as from *Sansevieria trifasciata* [25], *Murraya koenigii* [28], *Jatropha podagrica* [20], and *Mentha piperita* [29], for the production of ferrite compounds.

Terminalia catappa L. is a plant that is native to the Asian continent and is renowned for its diverse bioactivities. The plant is referred to as ketapang in Indonesia. The extract of *Terminalia catappa* leaves includes many bioactive compounds, including flavonoids, tannins, phenolics, kaempferol, and polyphenols [30, 31]. This substance is a reducing and capping agent to prevent the ferrite compounds from agglomerating [32].

In this study, *Terminalia catappa* leave extract was used to produce spinel ferrite $CdFe_2O_4$, which was then employed to photodegrade Methyl red dye. $CdFe_2O_4$ has a chemical stability, a low valence band position, strong oxidation characteristics, visible light absorption, and good magnetic properties [33]. The magnetic properties of $CdFe_2O_4$ make it an excellent reusable catalyst, as it can be easily separated from the solution using an external magnet. The optimization of the photodegradation process was determined using Response Surface Methodology (RSM) based on a Central Composite Design (CCD) with the variables of pH, Methyl red dye concentration, and irradiation time.

2. Experimental

2.1. Materials

The chemical reagents were sourced from Sigma Aldrich, including $Fe(NO_3)_3.9H_2O$, $(Cd(NO_3)\cdot 6H_2O$, Methyl red dye, HCl, and NaOH. The leaves of *Terminalia catappa* were acquired from Indralaya, Ogan Ilir district, Indonesia.

2.2. Preparation

The leaves of *Terminalia catappa* were purified and rinsed with distilled water, then air-dried for 2 days. The dried leaves are sliced into pieces measuring approximately (±1 cm). A total of 50 g of leaves were heated in 100 ml of distilled water for 90 minutes at a temperature ranging from 80 to 90 °C. After the leave extract has been cooled and filtered, it is finally ready to be utilized [29].

2.3. Synthesis of $CdFe_2O_4$

$Fe(NO_3)_3\cdot 9H_2O$ and $Cd(NO_3)_2\cdot 4H_2O$ were molar ratio of 2:1 dissolved in 50 ml of *Terminalia catappa* leave extract. The mixture was stirred at a speed of 500 rpm for 30 min. This mixture was placed inside an autoclave tube and subjected to a temperature of 180 °C for 2 h. The produced precipitate was rinsed with distilled water until it reached a pH of 7, then drying at a temperature of 100 °C in an oven for 2 h. Subsequently, the materials was pulverized using a mortar and then calcination at a temperature of 300 °C for 2 h.

2.4. Characterization

The crystal structure and crystallite size were determined by X-ray diffraction (XRD) analysis with a PANalytical X'Pert PRO instrument. The measurements were conducted in the 2θ range of 10–80° with a step size of 0.02° and Cu Kα radiation of 1.54056 Å. The functional group was examined using FTIR (Prestige 21 Shimadzu) with a KBr plate in the range of 4000–500 cm^{-1}. UV-DRS (Pharmaspec UV-1700) was employed to measure the absorbance and band gap within the range of 200–800 nm. The $CdFe_2O_4$ morphology was examined using a Scanning Electron Microscopy (JOEL JSM-6510 LA) equipped with energy-dispersive X-ray spectroscopy (EDS) to determine the elemental composition. The magnetic characteristics of $CdFe_2O_4$ were determined using a Vibrating Sample Magnetometer (Oxford Type 1.2 T). Brunauer-Emmett-Teller (BET) surface area analysis was determined using ASAP 2020. The UV-Vis Spectrophotometer (Type Ori-on Aquamate 8000) was used to measure the absorbance of the dye solution.

2.5. Photodegradation of Methyl red Dye

RSM is employed to identify the most favorable conditions for the degradation process. This is achieved by utilizing a CCD with three independent variables: the pH of the dye solution, the concentration of the dye, and the time of

 DOI: 10.15826/chimtech.2024.11.4.02

irradiation in response to the degradation efficiency of Methyl red dye. Table 1 shows the variation of the independent variables. A total of 20 experiments were conducted on the photodegradation process. The dye solution was 50 ml, with a catalyst dosage of 0.05 g/L. The experimental design was conducted using Design Expert 13. The light source utilizes a 300 W Xenon lamp that emits visible light radiation. The distance between the light source and the solution is 15 cm.

3. Result and Discussion

3.1. Characterization

XRD pattern of $CdFe_2O_4$ produced using *Terminalia catappa* leaves extract is shown in Figure 1. The distinctive peaks of $CdFe_2O_4$are observed at 2θ angles of 29.09°, 34.11°, 35.62°, 41.46°, 51.25°, 54.76°, and 60.01°, which correspond to the crystallographic planes (220), (311), (222), (400), (422), 511, and (440). These results support the cubic structure of $CdFe_2O_4$, according to JCPDS No. 22-1063. The average crystallite size of $CdFe_2O_4$, determined using the Scherrer equation, was 18.10 nm.

Typically, the peaks of metal oxides are below 1000 cm^{-1} due to the effects of intra-atomic vibrations [34]. Figure 2 illustrates the O–Fe–O stretching vibrations at a wave number of 567 cm^{-1}. Additionally, there is a low-intensity peak at a wave number of 848 cm^{-1}, which corresponds to the tetrahedral structure of Cd–Fe in $CdFe_2O_4$ [35]. The broad wave number at 3415 cm^{-1} suggests the existence of a phenolic group, which is corroborated by the absorption at 1165 cm^{-1}, indicating the presence of aromatic chemicals derived from plant extracts. Similarly, the peak at 1608 cm^{-1} is associated with stretching the C=C bond in the aromatic group [20].

The morphology of $CdFe_2O_4$ was examined through the analysis of secondary electron images. As depicted in Figure 3, the $CdFe_2O_4$ surface exhibits heterogeneity and tends to agglomerate. Figure 3 also displays the EDS mapping result, which reveals the distribution of elemental composition on the surface. The surface composition consists of Cd, Fe, O, and C, with relative percentages of 28.43%, 29.85%, 34.42%, and 7.30%. The element C is derived from the extract of *Terminalia catappa* leaves.

The band gap value of $CdFe_2O_4$ is determined by applying the T_{auc} as follows:

$$(\alpha h\nu)^{n} = A\left(h\nu - E_g\right), \quad (1)$$

where α is the absorption coefficient, A is the T_{auc} constant $h\nu$, is the photon energy and E_g is the band gap energy. The value of n depends on the type of optical transition that dominates the semiconductor, where n = 0.5 indicates a direct band gap and n = 2 is an indirect band gap [37].

The band gap energy is determined from a graph plot of $(\alpha h\nu)^2$ vs $h\nu$. The band gap energy of $NiFe_2O_4$ obtained is 1.78 eV. The band gap value closely aligns with the findings of other researchers, specifically 1.71 eV [19] and 2.08 eV [36]. Generally, spinel ferrite has a transition energy of less than 3 eV, which is the transfer of electrons from the d orbital. This transition is typically facilitated by spin-allowed processes [38].

Figures 4a and 4b display the absorbance and band gap values of $CdFe_2O_4$. Absorption peaks at wavelengths of 291, 378, and 704 nm were detected for $CdFe_2O_4$. It can be inferred that $CdFe_2O_4$ exhibits reactivity in the ultraviolet (UV) and visible parts of the electromagnetic spectrum. Additional studies indicate that $CdFe_2O_4$ produced using the hydrothermal technique exhibits identical absorption capabilities in the ultraviolet to visible spectrum [36].

The saturation magnetization (M_s) of $CdFe_2O_4$ was measured to be 28.34 emu/g, as depicted in Figure 5. The M_s value obtained in this investigation exceeded the findings of previous studies, specifically 11.3 emu/g [39].

Table 1 Range of variance for the independent variables.

Independent variables	Range levels		
	Low	Middle	High
pH	2	5	8
Concentration (mg/L)	10	25	40
Irradiation times (minutes)	30	75	120

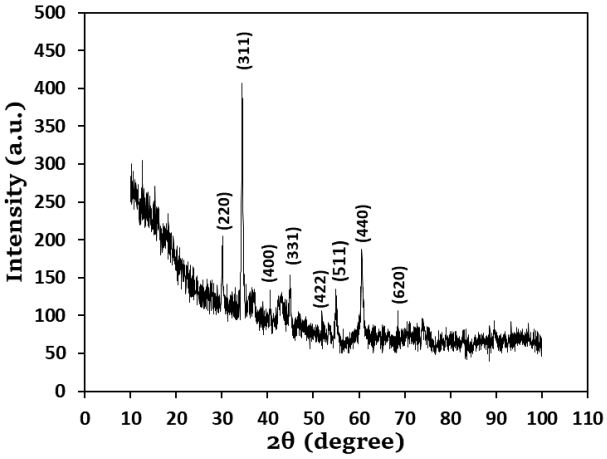

Figure 1 XRD pattern of $CdFe_2O_4$.

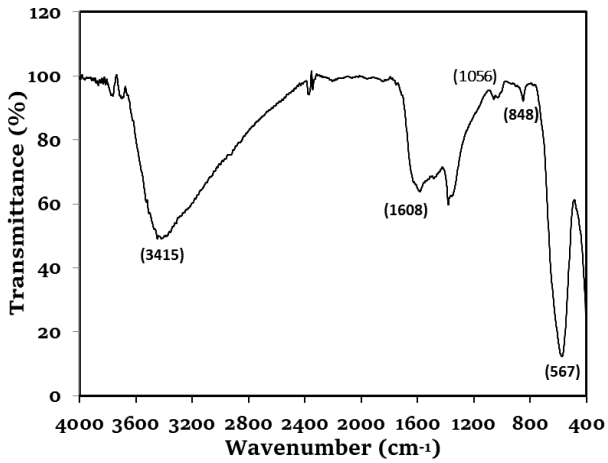

Figure 2 FTIR spectra of $CdFe_2O_4$.

 DOI: 10.15826/chimtech.2024.11.4.02

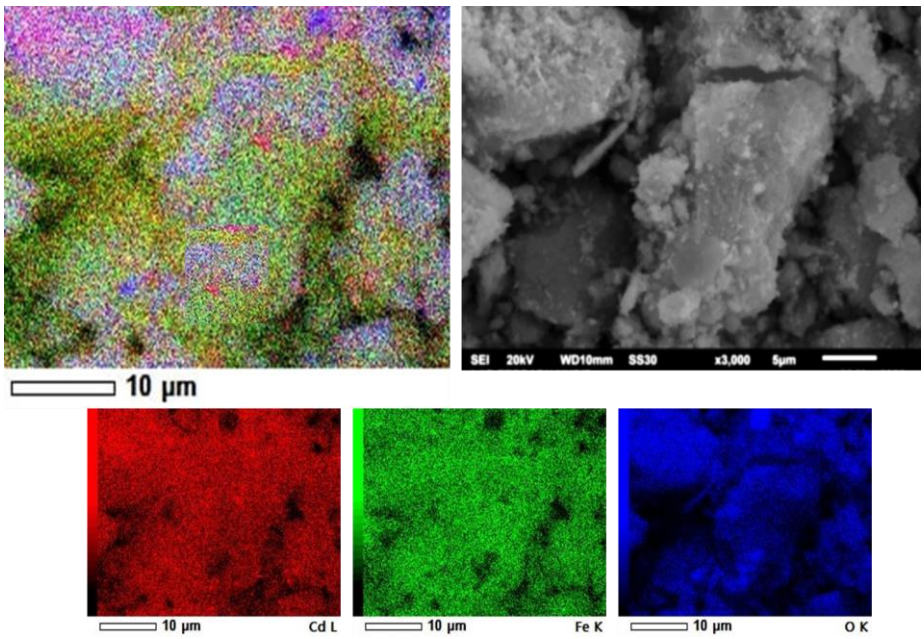

Figure 3 Morphology and elemental mapping of $CdFe_2O_4$.

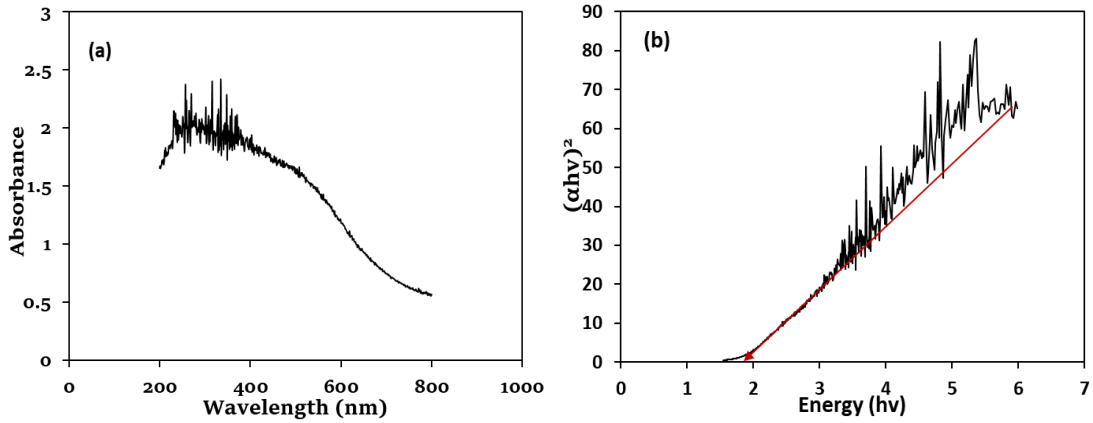

Figure 4 Graphs of DRS spectra (a) and $(\alpha h\nu)^2$ vs $h\nu$ (b).

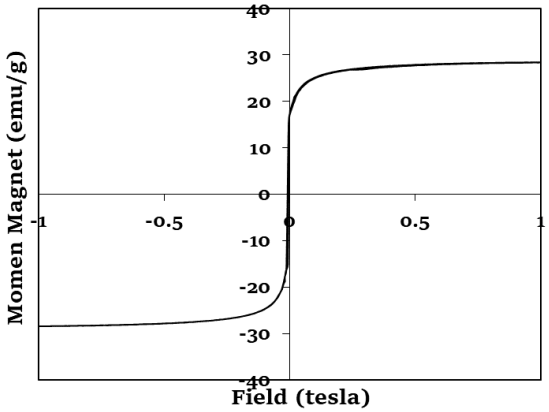

Figure 5 Magnetic hysteresis loops of $CdFe_2O_4$.

Figure 6 shows the specific surface of $CdFe_2O_4$ determined using N_2 adsorption/desorption isotherms. The curve indicates a typical type II isotherm. Total volume, pore size, and volume distribution were determined from BJH analysis. The total surface area of $CdFe_2O_4$ is 84.23 m^2/g, the pore volume is 0.252 cm^3/g, and the average pore size is 9.21 nm according to the BJH desorption curve. The BET surface area obtained in this study was greater than $CdFe_2O_4$ synthesized using the hydrothermal and pressure-impitation methods, respectively 67.21 m^2/g and 39 m^2/g [19, 39].

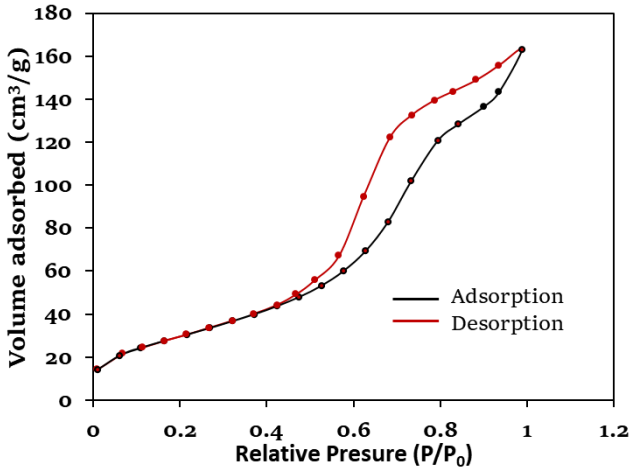

Figure 6 N_2 adsorption/desorption isotherms of $CdFe_2O_4$.

 DOI: 10.15826/chimtech.2024.11.4.02

3.2. CCD-based RSM optimization

The RSM is employed to determine the optimal conditions for the photodegradation of methyl red dye using $CdFe_2O_4$, with the solution pH (A), initial dye concentration (B), and irradiation duration (C) being varied. The experiment was designed based on CCD with 20 runs, as shown in Table 2.

Table 2 demonstrates that the actual dye removal percentage closely aligns with the predicted value, with an average difference of 2.85%. Analysis of Variance (ANOVA), provided in Table 3, complements the finding. The ANOVA analysis indicates that the quadratic model is appropriate for describing the photodegradation of Methyl red dye using $CdFe_2O_4$. The quadratic model's fit to the data is considered significant, with an *F*-value of 262.95 and a *p*-value (<0.0001) less than 0.05.

Table 2 Actual and predicted removal of Methyl red dye.

Run	A	B (mg/L)	C (min)	Photodegradation (%)	
				Actual (%)	Predicted (%)
1	8	10	30	79.56	77.58
2	5	25	120	83.32	83.58
3	5	25	75	89.23	88.418
4	5	25	30	81.1	77.728
5	2	40	120	88.95	89.24
6	2	25	75	87.43	91.59
7	5	25	75	88.46	88.41
8	5	25	75	88.32	88.41
9	5	25	75	88.67	92.22
10	8	40	120	81.34	68.89
11	2	10	120	96.56	97.66
12	5	25	75	88.46	92.22
13	8	10	120	78.70	77.32
14	5	25	75	88.70	88.41
15	5	10	75	90.22	92.39
16	8	25	75	84.32	77.04
17	2	40	30	85.20	84.89
18	2	10	30	77.10	78.71
19	5	40	75	95.80	99.93
20	8	40	30	95.68	79.69

Table 3 ANOVA analysis of experiment results.

Source	Sum of squares	df	Mean square	*F*-value	*p*-value
Model	583.37	9	65.04	262.95	<0.0001
A. pH	24.46	1	24.46	98.89	<0.0001
B. Concentration	61.65	1	61.65	249.26	<0.0001
C. Time	10.47	1	10.47	42.31	<0.0001
AB	41.72	1	41.72	168.69	<0.0001
AC	184.42	1	184.42	745.58	<0.0001
BC	106.51	1	106.51	430.60	<0.0001
A^2	13.23	1	13.23	53.50	<0.0001
B^2	67.15	1	67.15	271.47	<0.0001
C^2	94.39	1	94.39	381.61	<0.0001
Residual	2.47	10	0.2473		
Lack of Fit	1.95	5	0.3907	3.76	0.0863
Pure error	0.5198	5	0.1040		

The coefficient of determination (R^2) is a measure used to to evaluate the accuracy of a model. An R^2 value of 0.995 shows a strong correlation between the actual and the predicted value [40]. The results suggest that independent variables drive 99.5% of the dye removal, whereas only 0.5% remains unexplained by the model. Figure 7 illustrates the comparison between predicted and actual values.

The *p*-value serves to assess the interaction of independent variables, where a *p*-value < 0.05 indicates a statistically significant effect. The *p*-values for (A) pH, (B) concentration, and (C) irradiation duration are all <0.0001, indicating that these three variables have a statistically significant impact on the removal of dye (%). The interactions between variables *AB*, *AC*, and *BC* were considered significant because their *p*-values were less than 0.05. The *p*-values for A^2, B^2, and C^2 are all less than 0.0001, indicating a significant quadratic influence of these factors. This suggests that the response has a non-linear relationship with each variable.

The quadratic model describes the relationship between the independent variables (*A*, *B*, and *C*) as follows:

$$\text{Removal (\%)} = 59.401 + 3.315 \cdot A - 0.781 \cdot B + 0.769 \cdot C + 0.051 \cdot A \cdot B - 0.036 \cdot A \cdot C - 0.005 \cdot B \cdot C - 0.244 \cdot A^2 + 0.022 \cdot B^2 - 0.003 \cdot C^2 \quad (2)$$

The statistical assessment of the chosen model demonstrates favorable outcomes (Table 4). The discrepancy between the predicted R^2 value of 0.963 and the adjusted R^2 value of 0.992 is smaller than 0.2, suggesting that the model is highly accurate in predicting outcomes. In addition, the precision value of 53.874, which is greater than 4, indicates that the model's predictive power is adequate relative to the noise.

In order to identify the most favorable conditions and elucidate the relationships between variables, a response surface is generated utilizing the chosen quadratic model. 2D and 3D curves represent the regression equation when one of the variables is constant. The response surface can be used to characterize the influence of variables and ascertain the optimal conditions for dye removal.

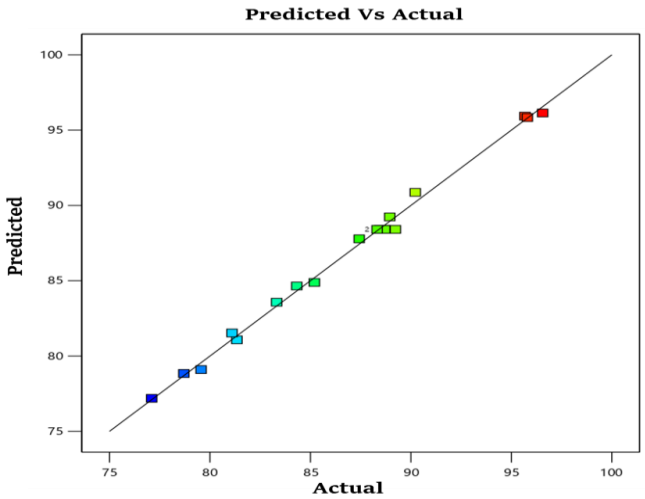

Figure 7 Predicted vs actual for photodegradation of Methyl red dye.

 DOI: 10.15826/chimtech.2024.11.4.02

Table 4 Statistical fit evaluation of the quadratic model.

Parameter	Value
Standard deviation	0.4973
Mean	86.86
C.V. %	0.5726
R^2	0.995
Adjusted R^2	0.992
Predicted R^2	0.963
Adeq Precision	53.874

Figure 8 reveals the effect of the independent variable on photodegradation efficiency. The relationship between solution pH and initial concentration demonstrates that achieving the optimal condition is more efficient when increasing the concentration within a specific pH range, specifically 6–7. The photodegradation efficiency in this instance approaches 94% when the concentration falls within the range of 30–40 mg/L, and the solution pH is maintained between 5 and 6.

The correlation between solution pH and irradiation time exhibits an ellipsoid surface, suggesting that the efficiency increases with longer irradiation time, but only up to a specific threshold beyond which it starts to decline. Optimal efficiency can be attained more rapidly by reducing the pH level, resulting in a shorter irradiation time. In this study, a pH level of around 5 yields a photodegradation efficiency of 85% within 40–50 min.

The relationship between the initial concentration and time demonstrates a saddle-shaped response surface. Increasing the concentration can enhance photodegradation efficiency, provided that the irradiation time is maintained within the range of 70 to 80 minutes. When the concentration falls between 34 and 40 mg/L and the period is between 70 and 80 minutes, a photodegradation efficiency of 95% is attained.

A separate investigation demonstrated a similar occurrence, wherein the optimal photodegradation efficiency for the Methyl red dye was achieved at a concentration of 35.94 mg/L within the range of 10–40 mg/L, utilizing a MgO catalyst [3]. It can be explained by the fact that when the concentration increases, the formation of hydroxyl radicals decreases, resulting in a decrease in photodegradation efficiency [28].

As for the solution pH, it affects the surface charge of the catalyst, interfacial electron transfer, and the mechanism for generating hydroxyl radicals [41]. At low pH levels, the degradation process is enhanced by the increased generation of hydroxyl radicals resulting from the interaction between hydroxide ions and the positive holes of the catalyst [4]. An elevation in pH level can lead to the recombination of electron and hole pairs, thereby diminishing the photocatalytic activity [42, 43].

The optimal conditions for photodegradation were achieved at a solution pH of 6.33, a dye concentration of 39.93 mg/L, and a time of 52.26 min. The desirability function was calculated to be 1.0, with a photodegradation efficiency of 96.56%. A desirability score of about implies that all targeted responses have been obtained (Figure 9).

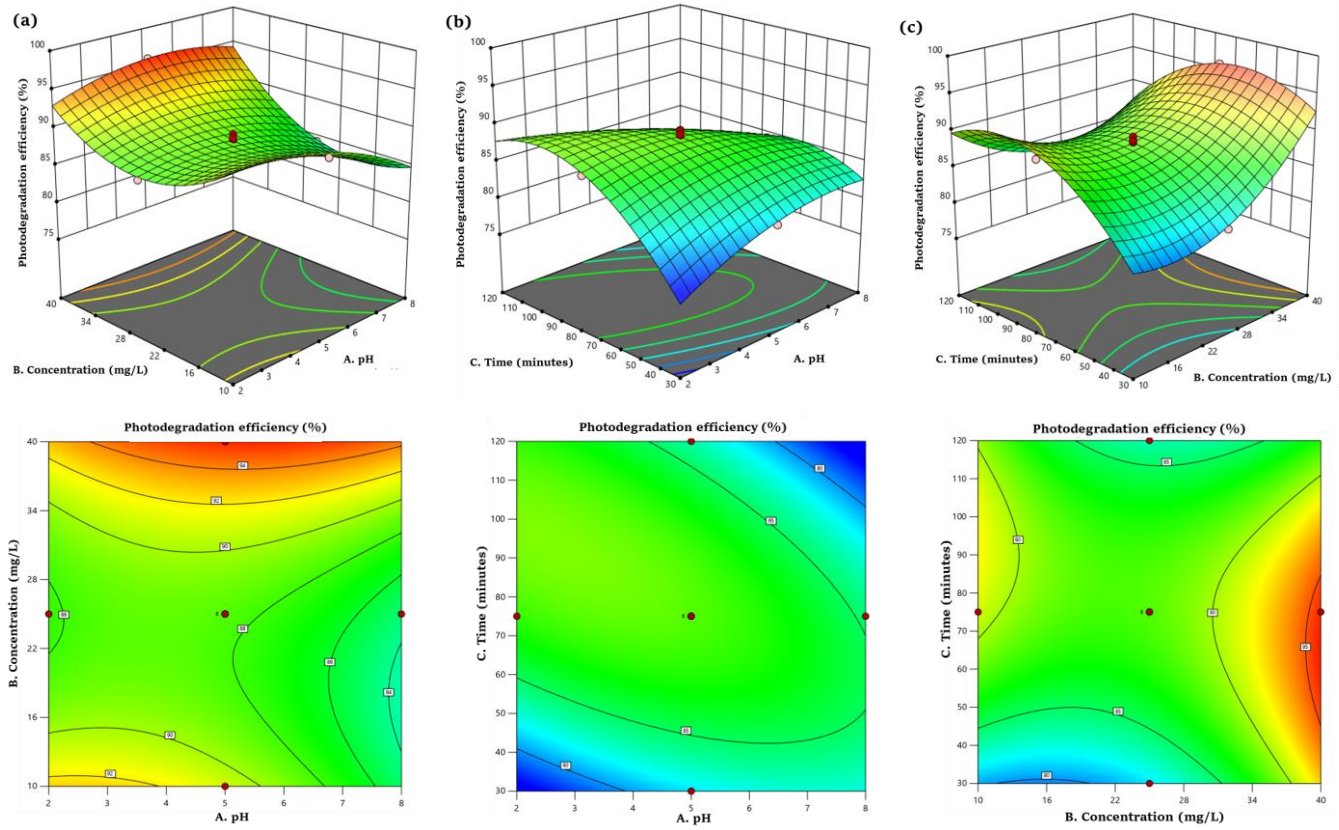

Figure 8 Response surface for intraction pH-concentration (a), pH-time (b) and concentration-time (c).

 DOI: 10.15826/chimtech.2024.11.4.02

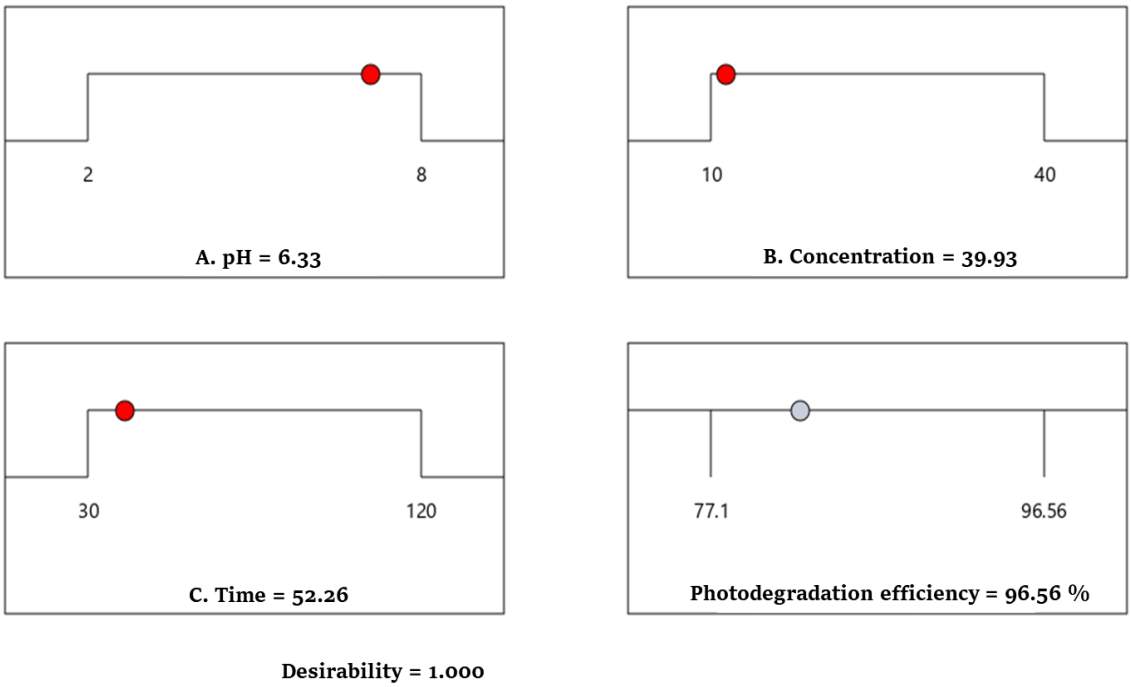

Figure 9 Desirability for optimization of three independent variables.

3.3. Kinetic and reusability

In this study, pseudo-first-order kinetics according to the Langmuir-Hinshelwood model was used to show the kinetic photodegradation of Methyl red dye using $CdFe_2O_4$. The pseudo-first-order equation is as follows [4]:

$$\ln\frac{C_0}{C} = -kt, \quad (3)$$

where C_0 is the initial concentration of methyl red dye, C is the concentration of Methyl red dye at any time (t). The correlation coefficient (R^2 = 0.98) is close to 1, indicating a positive correlation between $\ln\left(\frac{C_0}{C}\right)$ and irradiation time (t). The R^2 value clearly shows that the photodegradation conforms to pseudo-first-order kinetics. The value of k (the rate constant) obtained from the slope is 0.0622 min^{-1} (Figure 10). This k value is much greater than the other studies in Table 5.

The key feature of a catalyst is its ability to be reused without any loss in its activity. Following its use, the catalyst is cleansed using acetone and distilled water and subsequently dried at 80 °C for 3 h [47]. After being employed five times, the catalyst exhibits exceptional stability, with the photodegradation efficiency lowered to less than 5% (Figure 11). The decrease in activity may be attributed to blockages and a decrease in the number of active sites on the surface after several uses [26]. These findings suggest that the catalyst has promise for application in the treatment of industrial wastewater.

4. Limitations

The calcination process for the produced $CdFe_2O_4$ was conducted exclusively at 300 °C in this study. The temperature at which calcination occurs impacts the degree of crystallinity, the crystallite size, and the magnetic characteristics. Hence, further investigation is required to determine the optimal temperature for synthesizing $CdFe_2O_4$.

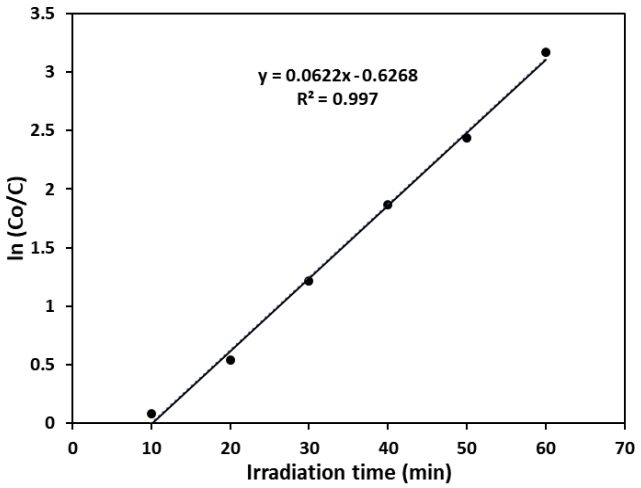

Figure 10 Kinetic model for photodegradation of Methyl red dye.

Table 5 The k value of Methyl red dye photodegradation utilizing various photocatalysts from previous experiments.

Catalyst	Experiment	k (min^{-1})	Ref.
MgO	MR = 35 mg/L, pH = 11.5,	0.0285	[3]
Sm–ZnO	MR = 5 mg/L, pH = 7	0.0167	[44]
Au–SiO_2	MR = 15 mg/L, pH = 2	0.0200	[45]
Y_2O_3–MgO/g-C_3N_4	MR = 30 mg/L, pH = 7	0.0267	[46]
PANI–SnO_2	MR = 20 mg/L, pH = 3	0.0240	[42]
$CdFe_2O_4$	MR = 40 mg/L, pH = 6.3	0.0622	In this study

 DOI: 10.15826/chimtech.2024.11.4.02

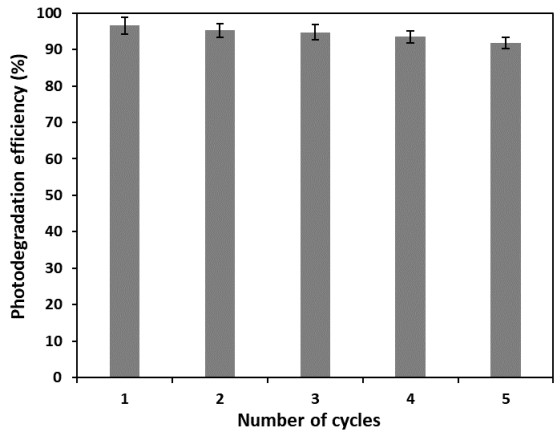

Figure 11 Photodegradation of Methyl red dye using $CdFe_2O_4$ during five degradation cycles.

5. Conclusions

The ferrite compound $CdFe_2O_4$ was synthesized using an extract from *Terminalia catappa* leaves. The $CdFe_2O_4$ obtained has a crystallite size of 18.10 nm, a band gap of 1.78 eV, BET surface area of 84.23 m^2/g, and exhibits magnetic properties, with a magnetic moment of 28.47 emu/g. This magnetic characteristic facilitates the retrieval of the catalyst following its utilization in the photodegradation process by employing a magnet instead of filtration. Photodegradation modeling of Methyl red dye using the CCD-based RSM method shows that the best fit is a quadratic model. The use of $CdFe_2O_4$ for the photodegradation of Methyl red dye has proven effective, achieving a photodegradation efficiency of 96.56% under optimal conditions: solution pH 6.33, dye concentration 39.93 mg/L, and an irradiation time of 52.26 minutes. The photodegradation kinetics follow a pseudo-first-order reaction with a rate constant (k) of 0.0622 min^{-1}. High catalyst stability allows the catalyst to be used repeatedly, with less than a 5% decrease in efficiency after five cycles. $CdFe_2O_4$ is expected to be a highly effective option for photocatalytic transformation due to its significant photodegradation activity.

• Supplementary materials

No supplementary materials are available.

• Funding

This research had no financial support.

• Acknowledgments

The author expresses gratitude to the Chemical Analysis and Instrumentation Laboratory, Faculty of Mathematics and Natural Sciences, Universitas Sriwijaya for its research facilities.

• Author contributions

Conceptualization: P.L.H.
Data curation: S.
Formal Analysis: P.L.H., E.S.Y.
Investigation: P.L.H., S.
Methodology: S., E.S.Y., B.R.A.
Supervision: P.L.H.
Writing – original draft: B.R.A., N.A.
Writing – review & editing: N.A., S.

• Conflict of interest

The authors declare no conflict of interest.

• Additional information

Author IDs:
Poedji Loekitowati Hariani, Scopus ID 55907597200;
Salni, Scopus ID 16553271400;
Eka Sri Yusmartini, Scopus ID 55668794300;
Nabila Apriani, Scopus ID 721868589005;
Bijak Riyandi Ahadito, Scopus ID 57212167604.

Websites:
Universitas Sriwijaya, https://unsri.ac.id/;
Universitas Muhammadiyah, https://umj.ac.id/;
Research Centre for Energy Conversion and Conservation (PRKKE), https://www.brin.go.id/en.

References

1. Wang Z, Hu M, Wang Q, Li L. Efficient and sustainable photocatalytic degradation of dye in wastewater with porous and recyclable wood foam@V_2O photocatalysts. J Clean Prod. 2022;332:1–10. doi:10.1016/j.jclepro.2021.130054
2. Raj RB, Umadevi M, Parimaladevi R. Enhanced photocatalytic degradation of textile dyeing wastewater under UV and visible light using ZnO/MgO nanocomposites as a novel photocatalyst. Part Sci Technol. 2020;38(7):812–820. doi:10.1080/02726351.2019.1616863
3. Ratnam MV, Karthikeyan C, Rao KN, Meena V. Magnesium oxide nanoparticles for effective photocatalytic degradation of methyl red dye in aqueous solutions: Optimization studies using response surface methodology. Mater Today Proc. 2020;26:2308–313. doi:10.1016/j.matpr.2020.02.498
4. Omotunde OI, Okoronkwo AE, Aiyesanmi AF, Gurgur E. Photocatalytic behavior of mixed oxide NiO/PdO nanoparticles toward degradation of Methyl red in water. J Photochem Photobiol A Chem. 2018;365:145–150. doi: 10.1016/j.jphotochem.2018.08.005
5. Kouakou LPM, Karidioula D, Manouan MRW, Pohan AGL, Cisse G, Konan LK, Andji-Yapi JY. Use of two clays from Cote ˆd'Ivoire for the adsorption of Methyl red from aqueous medium. Chem Phys Lett. 2020;810:1–8. doi:10.1016/j.cplett.2022.140183
6. Mahmoodi NM, Abdi J. Nanoporous metal-organic framework (MOF-199): Synthesis, characterization and photocatalytic degradation of Basic Blue 41. Microchem J. 2019;144:436–442. doi: 10.1016/j.microc.2018.09.033
7. Nandhini NT, Rajeshkumar S, Mythili S. The possible mechanism of eco-friendly synthesized nanoparticles on hazardous dyes degradation. Biocatal Agric Biotechnol. 2019;19:1–10. doi: 10.1016/j.bcab.2019.101138
8. Bouzid T, Grich A, Naboulsi A, Regti A, Tahiri AA, Himri ME, Haddad ME. Adsorption of Methyl red on porous activated carbon from agriculture waste: Characterization and

response surface methodology optimization. Inorg Chem Commun. 2023;158:1–12. doi:10.1016/j.inoche.2023.111544
9. Dessie Y, Tadesse S, Adimasu Y. Improving the performance of graphite anode in a microbial fuel cell via PANI encapsulated α-MnO_2 composite modification for efficient power generation and Methyl red removal. Chem Eng J Adv. 2022;10:1–13. doi:10.1016/j.ceja.2022.100283
10. Ndlovu LN, Ndlwana L, Mishra AK, Nxumalo EN, Mishra SB. Immobilizing palladium nanoparticles in beta-cyclodextrin-grafted graphene oxide modified polyvinylidene fluoride mixed matrix membranes for the removal of anionic azo dyes. Chem Eng Res Des. 2024;203:149–164. doi:10.1016/j.cherd.2024.01.044
11. Sharma K., Pandit S, Mathuriya AS, Gupta PK, Pant K, Jadhav DA. Microbial electrochemical treatment of Methyl red dye degradation using Co-Culture method. Water. 2023:15(56):1–17. doi:10.3390/w15010056
12. Anjali KP, Raghunathan R, Devi G, Dutta S. Photocatalytic degradation of Methyl red using seaweed mediated zinc oxide nanoparticles. Biocatal Agric Biotechnol. 2022;43:1–14. doi: 10.1016/j.bcab.2022.102384
13. Hariani PL, Salni S, Said M, Farahdiba R. Core-shell $Fe_3O_4/SiO_2/TiO_2$ magnetic modified Ag for the photocatalytic degradation of Congo red dye and antibacterial activity. Bull Chem React Eng Catal. 2023;18(2):315–330. doi:10.9767/bcrec.19275
14. Vishnu G, Singh S, Naik TSSK, Viswanath R, Ramamurthy PC, Bhadrecha P, Naik HSB, Singh J, Khan NA, Zahmatkesh S. Photodegradation of Methylene blue dye using light driven photocatalyst-green cobalt doped cadmium ferrite nanoparticles as antibacterial agents. J Clean Prod. 2023;404:1–15. doi:10.1016/j.jclepro.2023.136977
15. Yilkal DS, Abebe BG, Solomon GB. Optical photocatalytic degradation of Methylene blue using lignocellulose modified TiO_2. AJOAP. 2017;5(5): 55–58. doi:10.11648/j.ajop.20170505.12
16. Narang SB, Pubby K. Nickel Spinel Ferrites: A review. J Magn Magn Mater. 2021;519:1–58. doi:10.1016/j.jmmm.2020.167163
17. Zohrabi Y. Synthesis and application of magnetic ferrites (MFe_2O_4) in the removal of heavy metals from aqueous solutions: An updated review. Mater Sci Eng B. 2024;299: 1–14. doi:10.1016/j.mseb.2023.117024
18. Riyanti F, Nurhidayah, Purwaningrum W, Yuliasari N, Hariani, PL. $MgFe_2O_4$ magnetic catalyst for photocatalytic degradation of Congo red dye in aqueous solution under visible light irradiation. Environ Nat Resour J. 2023;21(4):322–332. doi:10.32526/ennrj/21/20230002
19. Douafer S, Lahmar H, Laouici R, Akika FZ, Trari M, Avramova I, Benamira M. Synthesis and characterization of $CdFe_2O_4$ nanoparticles: Application for the removal of Methyl green under solar irradiation. Mater Today Proc. 2023:35:1–10. doi:10.1016/j.mtcomm.2023.105630
20. Golthi V, Kommu J. An eco-friendly and sustainable method for producing Fe_3O_4 nanoparticles using *Jatropha podagrica* leaf extract for efficient dye degradation and antibacterial uses. Hybrid Adv. 2023;4:1–11. doi:10.1016/j.hybadv.2023.100110
21. Udhaya PA, Ahmad A, Meena M, Queen MAJ, Aravind M, Velusamy P, Almutairi TM, Mohammed AAA, Ali S. Copper Ferrite nanoparticles synthesised using a novel green synthesis route: Structural development and photocatalytic activity. J Mol Struct. 2023;1277:1–7. doi:10.1016/j.molstruc.2022.134807
22. Saraçoglu M, Mansoor M, Bakırdoven U, Arpalı H, Gezici UO, Timur S. Challenging the frontiers of superparamagnetism through strain engineering: DFT investigation and co-precipitation synthesis of large aggregated Fe_3O_4 (magnetite) powder. J Alloys Compd. 2023;968:1–10. doi: 10.1016/j.jallcom.2023.171895
23. Hariani PL, Said M, Rachmat A, Riyanti F, Pratiwi HC, Rizki WT. Preparation of $NiFe_2O_4$ nanoparticles by solution combustion method as photocatalyst of Congo red. Bull Chem React Eng Catal. 2021;16(3):481–490. doi:10.9767/bcrec.16.3.10848.481-490
24. Balasubramani V, Mowlika V, Sivakumar A, Sdran NA, Maiz F, Shkir M. Design and investigation of Sono-chemical synthesis of pure and Sn doped $CoFe_2O_4$ nanoparticles and their structural and magnetic properties. Inorg Chem Commun. 2023;155:1–6. doi:10.1016/j.inoche.2023.111015
25. Saridewi N, Utami DJ, Zulys A, Nurbayti S, Nurhasni, Adawiah, Putri AR, Kamal R. Utilization of Lidah mertua (*Sansevieria trifasciata*) extract for green synthesis of $ZnFe_2O_4$ nanoparticle as visible-light responsive photocatalyst for dye degradation. Case Stud Chem Environ Eng. 2024;9:1–9. doi:10.1016/j.cscee.2024.100745
26. Malik AR, Aziz MH, Atif M, Irshad MS, Ullah M, Gia TN, Ahmed H, Ahmad S, Botmart T. Lime peel extract induced $NiFe_2O_4$ NPs: Synthesis to applications and oxidative stress . mechanism for anticancer, antibiotic activity. J Saudi Chem Soc. 2022;26:1–11. doi:10.1016/j.jscs.2022.101422
27. Makofane A, Motaung DE, Hintsho-Mbita NC. Green synthesis of silver deposited on copper ferrite nanoparticles for the photodegradation of dye and antibiotics. Appl Surf Sci. 2024;21:1–15. doi:10.1016/j.apsadv.2024.100601
28. Alamier WM, Hasan N Nawaz MDS, Ismail KS, Shkir M, Malik MA, OteeF MDY. Biosynthesis of $NiFe_2O_4$ nanoparticles using *Murayya koenigii* for photocatalytic dye degradation and antibacterial application. J Mater Res Technol. 2023;22:1331–48. doi:10.1016/j.jmrt.2022.11.181
29. Kalita C, Boruah PK, Das MR, Saikia P. Facile green synthesis of nickel-ferrite-rGO ($NiFe_2O_4$/rGO) nanocomposites for efficient water purification under direct sunlight. Inorg Chem Commun. 2022;146:1–10. doi:10.1016/j.inoche.2022.110073
30. Devadiga A, Shetty V, Saidutta MB. Highly stable silver nanoparticles synthesized using *Terminalia catappa* leaves as antibacterial agent and colorimetric mercury sensor. Mater Lett. 2017;207:66–77. doi: 10.1016/j.matlet.2017.07.024
31. Mantaring, SDA, Santos JRKD, Estrella R., Jose JPG, Castro IJL, Bigol UG, Guzman JPMD. *Terminalia catappa* L. leaf extract interferes with biofilm formation of *Vibrio parahaemolyticus* and enhances immune response of *Penaeus vannamei* against acute hepatopancreatic necrosis disease (AHPND). Aquac. 2024;579:1–10. doi:10.1016/j.aquaculture.2023.740266
32. Singh J, Dutta T, Kim K, Rawat M, Samddar, P, Kumar P. Green synthesis of metals and their oxide nanoparticles: applications for environmental remediation. Nanobiotechnol. 2018;16(84):1–24. doi:10.1186/s12951-018-0408-4
33. Sharma Y, Sharma N, Rao GVS, Chowdari BVR. Li-storage and cycling properties of spinel, $CdFe_2O_4$, as an anode for lithium ion batteries. Bull Mater Sci. 2009;32:295–304. doi:10.1007/s12034-009-0043-7
34. Paul S, Shakya AK, Ghosh PK. Bacterially-assisted recovery of cadmium and nickel as their metal sulfide nanoparticles from spent Ni–Cd battery via hydrometallurgical route. J Environ Manage. 2020;16:1–10. doi:10.1016/j.jenvman.2020.110113
35. Varpe AS, Deshpande MD., Tope DR, Borhade AV. Enhanced photocatalytic performance of $CdFe_2O_4/Al_2O_3$ nanocomposite for dye degradation. Environ Sci Pollut Res. 2023;30:52549–60. doi:10.1007/s11356-022-24834-4
36. Keerthana SP, Yuvakkumar R, Ravi G, Arunmetha S, Thambidurai M, Velauthapillai D. Magnetically separable rare earth metal incorporated $CdFe_2O_4$ photocatalyst for degradation of cationic and azo dyes. J Mol Struct. 2024;1302:1–14. doi:10.1016/j.molstruc.2024.137479
37. Wan Y, Chen J, Zhan J, Ma Y. Facile synthesis of mesoporous $NiCo_2O_4$ fibers with enhanced photocatalytic performance for the degradation of Methyl red under visible light irradiation. J Environ Chem Eng. 2018;6(5):6079–87. doi:10.1016/j.jece.2018.09.023
38. Ravindra, A.V., Chandrika, M., Rajesh, C. P Kollu P, Ju S, Ramarao SD. Simple synthesis, structural and optical properties

of cobalt ferrite nanoparticles. Eur Phys J Plus. 2019;134(296). doi: 10.1140/epjp/i2019-12690-2
39. Wang H, Ji P, Zhang Y, Zhang Y. Synthesis of magnetic Z-scheme $MoS_2/CdFe_2O_4$ composite for visible light induced photocatalytic degradation of tetracycline. Mater Sci Semicond Process. 2022;152:1–11. doi:10.1016/j.mssp.2022.107075
40. Murshed MK, Dursun AY, Dursun G. Application of response surface methodology on photocatalytic degradation of Astrazon orange G dye by ZnO photocatalyst: Internal mass transfer effects. Chem Eng Res Des. 2022;188:27–38. doi:10.1016/j.cherd.2022.09.038
41. Fan H, Jiang T, Li H, Wang D, Wang L, Zhai J, He D, Wang P, Xie T. Effect of $BiVO_4$ Crystalline phases on the photoinduced carriers behavior and photocatalytic activity. J Phys Chem. 2012; 116(3):2425–30. doi:10.1021/jp206798d
42. Kanwal A, Rehman MU, Sattar R, Thebo KH, Kazi M. Highly efficient tin oxide and polyaniline-tin-oxide nanostructured materials for photocatalytic degradation of organic dyes. J Mol Struct. 2024;1312:1–12. doi:10.1016/j.molstruc.2024.138454
43. Nethravathi PC., Shruthi GS, Suresh D, NagabhushanaH, Sharma SC. *Garcinia Xanthochymus* mediated green synthesis of ZnO nanoparticles: photoluminescence, photocatalytic and antioxidant activity studies. Ceram Int. 2015;41(7):8680–8687. doi:10.1016/j.ceramint.2015.03.084
44. Anjali KP, Raghunathan R, Devi G, DuttaS. Photocatalytic degradation of Methyl red using seaweed mediated zinc oxide nanoparticles. Biocatal Agric Biotechnol. 2022;43:1–13. doi:10.1016/j.bcab.2022.102384
45. Galenda A, Crociani L, El Habra N, Favaro M, Natile MM, Rossetto G. Effect of reaction conditions on Methyl red degradation mediated by boron and nitrogen doped TiO_2. Appl Surf Sci. 2014;314:919–30. doi:10.1016/j.apsusc.2014.06.175
46. Alharbi AA, Aldaghri O, El-Badry BA, Ibnaouf KH, Alfadhi F, Albadri A, Ajmed AH, Modwi A. Degradation of Methyl Red (MR) dye via fabricated Y_2O_3–MgO/g-C_3N_4 nanostructures: Modification of band gap and photocatalysis under visible light. Opt Mater Express. 2024;152:1–11. doi:10.1016/j.optmat.2024.115443
47. Ch V, Sandupatla R, Lingareddy E, Raju D. One-pot synthesis of imines by direct coupling of alcohols and amines over magnetically recoverable $CdFe_2O_4$ nanocatalyst. Mater Lett. 2021;302:1–6. doi:10.1016/j.matlet.2021.130417

 DOI: 10.15826/chimtech.2024.11.4.02